Supplemental Materials for "Magnetic properties of Os(IV) complexes: an *ab initio* analysis†"

Liviu Ungur,[1] Katharina Pallitsch,[2] Zeid A. AlOthman,[3] Abdullah A. S. Al-Kahtani,[3] Vladimir B. Arion,[4] and Liviu F. Chibotaru[2]

[1] *Department of Chemistry, National University of Singapore, Block S8 Level 3, 3 Science Drive 3, 117543, Singapore.*
[2] *Theory of Nanomaterials Group, KU Leuven, Celestijnenlaan 200F, B-3001 Leuven, Belgium*
[3] *Chemistry Department, College of Science, King Saud University, P.O. Box 2455, Riyadh 11451, Saudi Arabia.*
[4] *University of Vienna, Institute of Inorganic Chemistry, Währinger Strasse 42, A-1090 Vienna, Austria.*

(Dated: July 23, 2021)

CONTENTS

I. COMPUTATIONAL DETAILS

In order to test the validity of our computational approach applied for the study of the trans-$[Os^{IV}Cl_4(\kappa N_1\text{-Hind})_2]$ complex, we have performed similar *ab initio* calculations on the model $[Os^{IV}Cl_6]^{2-}$ structures: octahedral $[Os^{IV}Cl_6]^{2-}$ (**1**) and axially compressed $[Os^{IV}Cl_6]^{2-}$ (**2**).

The structural parameters of the calculated compounds:

- octahedral $[Os^{IV}Cl_6]^{2-}$ (**1**). R(Os-Cl) = 2.341695 $\mathring{A}$.
- axially compressed $[Os^{IV}Cl_6]^{2-}$ (**2**). R_{axial}(Os-Cl)= 2.04957 $\mathring{A}$; $R_{equatorial}$ (Os-Cl)= 2.341695 $\mathring{A}$.

The contractions of the employed basis sets are given in Table S1. Three active spaces were considered in the CASSCF method:

1. **AS0** = CAS (4 el. in 5 orb.) – the minimal active space for a $5d^4$ electronic configuration.
2. **AS1** = CAS (8 el. in 12 orb.)
3. **AS2** = CAS (14 el. in 13 orb.)

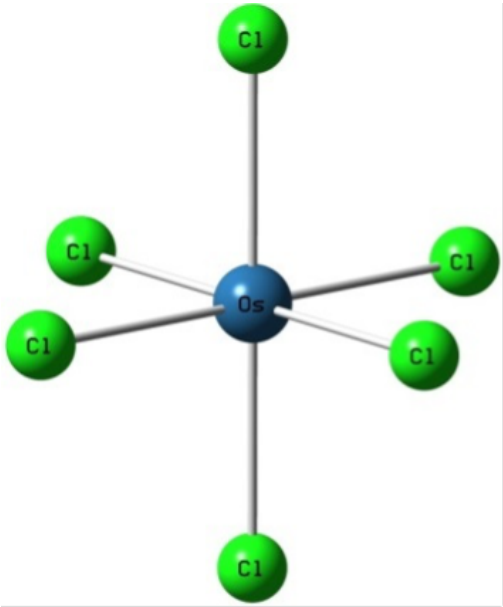

FIG. S1. Structure of the investigated $[Os^{IV}Cl_6]^{2-}$ anions. R(Os-Cl)= 2.341695 Å.

II. INFLUENCE OF THE BASIS SET ON THE COMPUTED LOW-LYING ENERGY STATES

TABLE S1. Contractions of the employed basis sets

Atom	**Basis A**	**Basis B**	**Basis C**
Os	7s6p4d2f	8s7p5d3f2g1h	9s8p6d4f3g2h
Cl	4s3p1d	5s4p2d	5s4p2d1f
N,C (close)	3s2p	4s3p2d	4s3p2d1f
N,C (distant)	3s2p	3s2p1d	3s2p1d
H (close)	2s	2s1p	3s2p1d
H (distant)	2s	2s1p	3s1p

TABLE S2. Energies of the calculated spin-orbit states, in function of the basis set and active space for the octahedral $[Os^{IV}Cl_6]^{2-}$ (**1**), in cm^{-1}.

AS1			**AS2**			**AS3**		
A	**B**	**C**	**A**	**B**	**C**	**A**	**B**	**C**
0.0	0.0	0.0	0.0	0.0	0.0	0.0	0.0	0.0
3206.7	3109.7	3129.0	3096.8	3035.0	3048.4	3003.6	2941.2	2948.8
3206.7	3109.7	3129.0	3096.8	3035.0	3048.4	3003.6	2941.2	2948.8
3206.7	3109.7	3129.0	3096.8	3035.0	3048.4	3003.6	2941.2	2948.8
6126.7	6005.8	6043.4	5973.3	5870.1	5890.2	5751.8	5654.8	5670.9
6126.7	6005.8	6043.4	5973.3	5870.1	5890.2	5751.8	5654.8	5670.9
6143.3	6047.0	6085.0	5985.9	5883.2	5942.6	5751.8	5654.8	5670.9
6143.3	6047.0	6085.0	5985.9	5883.2	5942.6	5772.7	5673.3	5689.2
6143.3	6047.0	6085.0	5985.9	5883.2	5942.6	5772.7	5673.3	5689.2

From Table S2 we notice the small decrease ($\approx$100 cm^{-1}) of the excitation energies of the $J = 1$ and $J = 2$ spin-orbital multiplets when the basis set increases (A$\rightarrow$C). At the same time we see a stronger decrease ($\approx$200 cm^{-1} for $J = 1$ and $\approx$ 400 cm^{-1} for $J = 2$) of the excitation energies when the active space is enlarged (AS0$\rightarrow$AS2).

TABLE S3. Energies of the calculated spin-orbit states, in function of the basis set and active space for the axially compressed octahedral $[Os^{IV}Cl_6]^{2-}$ (**2**), in cm^{-1}.

AS1			**AS2**			**AS3**		
A	**B**	**C**	**A**	**B**	**C**	**A**	**B**	**C**
0.0	0.0	0.0	0.0	0.0	0.0	0.0	0.0	0.0
2216.0	2108.8	2112.9	2213.8	2138.6	2137.9	2194.9	2152.6	2157.9
2216.0	2108.8	2112.9	2213.8	2138.6	2137.9	2194.9	2152.6	2157.9
5080.2	5218.6	5259.3	4725.9	4807.5	4829.2	4569.6	4564.0	4571.1
6275.8	6318.6	6357.8	5969.2	5964.2	5980.5	5932.1	5887.1	5898.8
6670.7	6751.0	6795.5	6507.4	6543.5	6564.8	6170.4	6130.2	6142.1
6830.6	6929.8	6976.6	6507.4	6543.5	6564.8	6299.3	6269.9	6287.1
6830.6	6929.8	6976.6	6619.0	6627.5	6640.6	6321.4	6293.0	6305.8
7045.2	7113.3	7156.4	6731.2	6749.6	6771.4	6321.4	6293.0	6305.8

The excited $J = 1$ spin-orbital multiplet of the axially compressed octahedral $[Os^{IV}Cl_6]^{2-}$ (**2**), is split in a spin-orbital doublet and a singlet. From Table S4 we notice the very small energy change of the excited doublet state, while the energy of the singlet is almost not varying with the increase of the basis set, while it is strongly lowered upon increase of the active space (up to ≈700 cm^{-1} for basis C). The relative energies of the higher excited $J = 2$ follow the same trend: they are mostly affected by the size of the active space, rather than by the size of the basis set.

III. INFLUENCE OF THE NUMBER OF ROOTS MIXED BY SPIN-ORBIT COUPLING ON THE COMPUTED LOW-LYING ENERGY STATES

The number of roots mixed by the spin orbit coupling in RASSI has an important effect on the resulting energy spectrum. Choosing an optimal number of states to be optimized is of great importance on the feasibility of the calculation: when the active space and the number of roots are both large, then the time for the CASSCF optimization grows exponentially. The same is true for the CASPT2 treatment.

In order to test the influence of the number of roots mixed by spin-orbit coupling we have made a series of calculation mixing:

- **NR1** – three spin triplet states (the octahedral $^3T_1$ term)
- **NR2** – **NR1** + ^5E, $^1T_1$, ^1E and ^1A terms
- **NR3** – 5 quintets, 45 triplets and 50 singlets, i.e. all ligand field states arising from **AS1**

All energies presented below have been obtained with the basis A, active space AS0.

We notice a strong change of the low-lying energy spectrum when more spin states (alongside with the ground $^3T_1$ term) are mixed by the spin-orbit coupling. As expected, we notice a slight decrease in the weight of the $^3T_1$ roots in the nine lowest spin-orbitals, not affecting, however, their dominant contribution for these states. We notice also that mixing all ligand field states (**NR3**) does not induce a strong departure from **NR2**. From this we can conclude that the **NR2** is the most optimal number of roots to be mixed for the studied complexes. We notice here the small splitting of the excited $J = 2$ spin-orbital multiplet in **NR2** and **NR3** cases. This splitting is a natural result of the O_h point group symmetry, which cannot preserve the degeneracy larger than 3. This splitting does not occurs due to different level of admixture of higher spin states to the states forming $J = 2$, thus causing their splitting. The axial ligand field created by the closer *Cl* atoms in **2** is similar in its nature to the field created by *N* atoms in trans-$[Os^{IV}Cl_4(\kappa N_1\text{-Hind})_2]$. Therefore, we considered **NR2** to be optimal for an accurate description of low-lying states in trans-$[Os^{IV}Cl_4(\kappa N_1\text{-Hind})_2]$ compound.

TABLE S4. Energies of the calculated spin-orbit states, in function of the number of roots mixed by spin-orbit coupling., in cm^{-1}.

O_h-$[Os^{IV}Cl_6]^{2-}$, 1			**axially-compressed $[Os^{IV}Cl_6]^{2-}$, 2**		
NR1	**NR2**	**NR3**	**NR1**	**NR2**	**NR3**
0.0	0.0	0.0	0.0	0.0	0.0
1596.0	3206.7	3456.9	1595.9	2216.0	2304.0
1596.0	3206.7	3456.9	1596.0	2216.0	2304.0
1596.0	3206.7	3456.9	1596.0	5080.2	5252.5
4788.0	6126.7	6198.5	4787.9	6275.8	6366.7
4788.0	6126.7	6198.5	4787.9	6670.7	6389.8
4788.0	6143.3	6198.5	4788.1	6830.6	6761.2
4788.0	6143.3	6265.9	4788.1	6830.6	6861.3
4788.0	6143.3	6265.9	4788.1	7045.2	6861.3
Average weight of the $^3T_1$ roots in the above spin-orbital states (in %)					
100	90	85	100	89	84

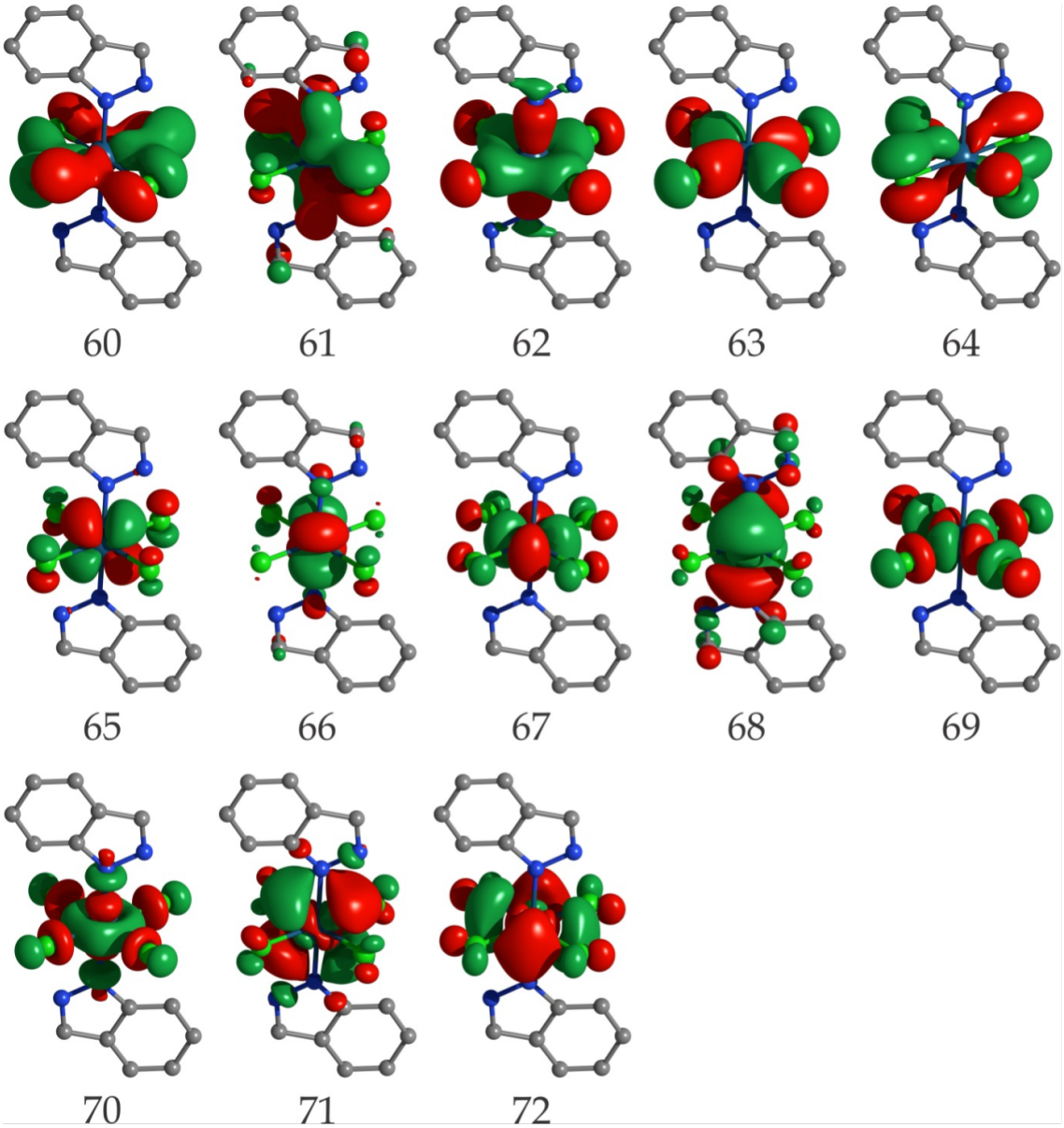

FIG. S2. Optimized active orbitals in the largest computational approximation. Orbitals 60-64 are ligand type orbitals having large contribution from Os $5d$ functions; orbitals 65-67 form the Os t_{2g} shell, while the orbitals 69 and 70 form the e_g shell; the remaining orbitals 68, 71,72 are the "double shell" of the orbitals from the t_{2g} shell. (Basis C, AS2)

IV. THE LIGAND-FIELD MODEL OF THE $^3T_1$ TERM

To get more insight into the calculated magnetic properties of Os(IV) complexes, we confront the results obtained from *ab initio* calculations with their ligand-field description within the minimal model, including only the ground term $^3T_1$, which entails the largest (first-order) spin-orbit coupling.

The spin-orbit coupling in the ground term $^3T_1$ is of the form[1]: $k\lambda_0\tilde{\boldsymbol{L}}\cdot\boldsymbol{S}$, where $\lambda_0 = \pm\zeta_{Os_{IV}} = 4000\text{cm}^{-1}$ is the spin-orbit coupling constant for Os(IV) ion and k is the orbital reduction factor due to covalence effects.[1, 2] The sign of λ_0 defines the order of the $\tilde{J}$ multiplets. When $\lambda_0 > 0$ the state with $\tilde{J} = 0$ will be the lowest in energy, while $\lambda_0 < 0$ stabilises the $\tilde{J} = 2$ in the ground state. In the present case, there are four electrons in the t_{2g} electronic shell, i.e., this shell is more than half-filled, which means that λ_0 is negative.[1, 3] On the other hand, the matrix elements of the effective $\tilde{L} = 1$ have opposite signs compared to matrix elements of a true orbital momentum $L = 1$. This can be summarized as follows:

$$\lambda = \xi k\lambda_0, \tag{S1}$$

where ξ is the proportionality factor (-1) between matrix elements of a true orbital momentum $L = 1$ and the matrix elements of the effective $\tilde{L} = 1$.[1] Therefore, absorbing this change of sign into the effective spin-orbit coupling constant, λ remains positive, and the ground multiplet is $\tilde{J} = 0$.

The splitting pattern of the low-lying levels in this case can be modelled within the ligand field theory by a model Hamiltonian comprising two interaction: i) the spin-orbit coupling between the $S = 1$ and the octahedral $\tilde{L} = 1$, as discussed above, leading to the $|\tilde{J}, M_{\tilde{J}}\rangle$ multiplets, and ii) the ligand-field splitting of the $^3T_1$ term, described by the axial splitting Δ_t and rhombic splitting Δ_e parameters. The Hamiltonian has the form:

$$\hat{H} = \lambda\tilde{\boldsymbol{L}}\cdot\boldsymbol{S} + \Delta_t(\tilde{L}_Z^2 - \frac{\tilde{L}(\tilde{L}+1)}{3}) + \Delta_e(\tilde{L}_X^2 - \tilde{L}_Y^2) \tag{S2}$$

The eigenfunctions of the total momentum $|\tilde{J}, M_{\tilde{J}}\rangle$ can be easily constructed as a linear combination of $|\tilde{L}, M_{\tilde{L}}\rangle|S, M_S\rangle$ basis states multiplied by the corresponding Clebsch-Gordan coupling coefficients, (Eq. S1).[4] The matrix of the ligand-field Hamiltonian (Eq. S2) written in the coupled basis, Eq. S1 is given in Eq. S2. Diagonalization of the ligand-field Hamiltonian (Eqs. S2), S2) gives the eigenenergies and eigenvectors, corresponding to mixing of the $|\tilde{J}, M_{\tilde{J}}\rangle$ multiplets when low-symmetry ligand field (last term in Eq. S2) is applied.

A. Magnetic properties of $\tilde{J}$ multiplets

The matrices of the spin (S_α) and orbital (L_α) momenta written in the spin-orbit coupled basis (Eq. S1) are given in SI (Tables S3 and S4). From them, the matrix of total magnetic momentum is given as follows:

$$\mu_\alpha = -\mu_B(\xi k\tilde{L}_\alpha + g_e S_\alpha), \tag{S3}$$

where g_e is the electronic g factor (≈ 2.00232), μ_B is the Bohr magneton.

These matrices can be rewritten in the basis which diagonalises the ligand-field Hamiltonian (Eq. S2):

$$\begin{aligned} S_\alpha^{'} &= U^\dagger S_\alpha U \\ L_\alpha^{'} &= U^\dagger L_\alpha U \\ \mu_\alpha^{'} &= U^\dagger \mu_\alpha U \end{aligned} \tag{S4}$$

where U is the unitary matrix diagonalizing the ligand-field Hamiltonian (Eq. S2). From matrix elements of $\mu_\alpha^{'}$, the g tensor can be straightforwardly calculated.[5]

B. g-factors for the $\tilde{J}$ multiplets of octahedral complexes

Within the employed ligand-field model specific to the $^3T_1$ term, the Zeeman Hamiltonian has the form:

$$\hat{H}_{Zee} = \mu_B(\xi k\tilde{\boldsymbol{L}} + g_e\boldsymbol{S})\cdot\boldsymbol{B}, \tag{S5}$$

where $\boldsymbol{B}$ is the magnetic field. The Zeeman splitting of $|\tilde{J}, M_{\tilde{J}}\rangle$ multiplets is obtained as:

$$E_{\tilde{J},M_{\tilde{J}}} = \mu_B[\xi k\langle \boldsymbol{L}\rangle_{M_{\tilde{J}}} + g_e\langle \boldsymbol{S}\rangle_{M_{\tilde{J}}}] \cdot \boldsymbol{B}, \tag{S6}$$

where $\langle \boldsymbol{L}\rangle_{M_{\tilde{J}}}$ and $\langle \boldsymbol{S}\rangle_{M_{\tilde{J}}}$ are expectation values of orbital and spin momenta operators in the corresponding $M_{\tilde{J}}$ state. For projections along quantization axis we obtain:

$$\begin{aligned}\langle \hat{S}_Z\rangle_{M_{\tilde{J}}} &= \frac{\langle \tilde{\boldsymbol{J}}\cdot\boldsymbol{S}\rangle}{\tilde{\boldsymbol{J}}^{\boldsymbol{2}}} M_{\tilde{J}} = \frac{\tilde{J}(\tilde{J}+1)+S(S+1)-\tilde{L}(\tilde{L}+1)}{2\tilde{J}(\tilde{J}+1)} M_{\tilde{J}} \\ \langle \hat{L}_Z\rangle_{M_{\tilde{J}}} &= \frac{\langle \tilde{\boldsymbol{J}}\cdot\boldsymbol{L}\rangle}{\tilde{\boldsymbol{J}}^{\boldsymbol{2}}} M_{\tilde{J}} = \frac{\tilde{J}(\tilde{J}+1)-S(S+1)+\tilde{L}(\tilde{L}+1)}{2\tilde{J}(\tilde{J}+1)} M_{\tilde{J}}\end{aligned} \tag{S7}$$

Substituting Eq. S7 in Eq. S6 yields:

$$E_{\tilde{J},M_{\tilde{J}}} = \mu_B \frac{\xi k[\tilde{J}(\tilde{J}+1)-S(S+1)+\tilde{L}(\tilde{L}+1)]+g_e[\tilde{J}(\tilde{J}+1)+S(S+1)-\tilde{L}(\tilde{L}+1)]}{2\tilde{J}(\tilde{J}+1)} M_{\tilde{J}} \cdot \boldsymbol{B}, \tag{S8}$$

from which the g factor for each manifold is derived:

$$g_{\tilde{J}} = 1 + \frac{(\xi k+g_e-2)\tilde{J}(\tilde{J}+1)+(g_e-\xi k)S(S+1)+(\xi k-g_e)\tilde{L}(\tilde{L}+1)}{2\tilde{J}(\tilde{J}+1)} \tag{S9}$$

For the particular case $\xi = -1$, $k = 1$, and $g_e = 2$, the expression Eq.S9 becomes:

$$g_{\tilde{J}} = 1 + \frac{-\tilde{J}(\tilde{J}+1)-3S(S+1)+3\tilde{L}(\tilde{L}+1)}{2\tilde{J}(\tilde{J}+1)} \tag{S10}$$

Substituting $\tilde{L} = 1$ and $S = 1$, relevant to the present case, into Eq.S10 we obtain:

$$g_{\tilde{J}} = 1 + \frac{\xi k}{2} \tag{S11}$$

One infers from Eq.S11 that the value of the g-factors predicted by the employed ligand-field model are the same for both $\tilde{J}$ manifolds, $g_1 = g_2$. In usual cases, when $\xi = 1$, the orbital reduction factor k is responsible for a decreasing of the g factors of both multiplets from their non-covalent value of $\frac{3}{2}$, while in the present case, with $\xi = -1$, the orbital reduction factor k is responsible for their *increasing* from their non-covalent value of $\frac{1}{2}$.

V. *AB INITIO* STUDY OF THE OCTAHEDRAL $[OS^{IV}CL_6]^{2-}$ ANION

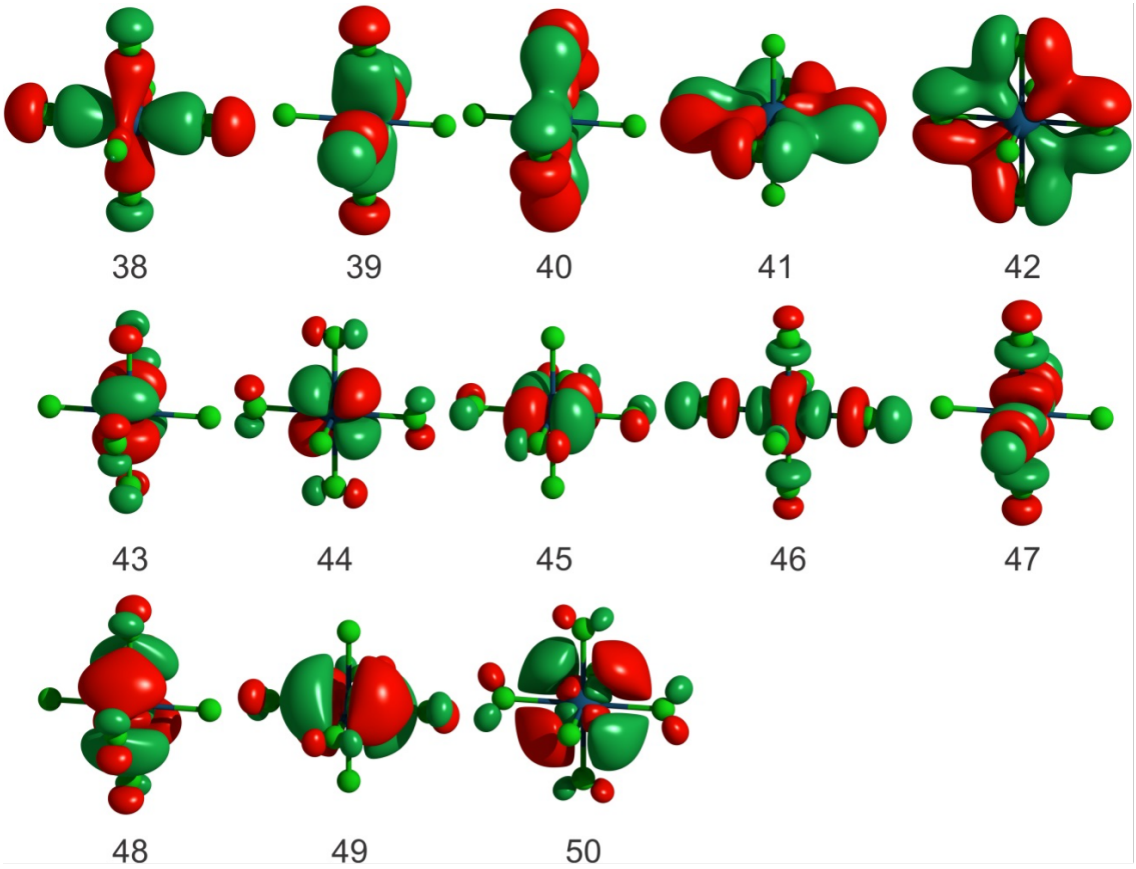

FIG. S3. Active orbitals for octahedral $[Os^{IV}Cl_6]^{2-}$ in the largest computational model: Basis C, AS2 (Basis C, AS2)

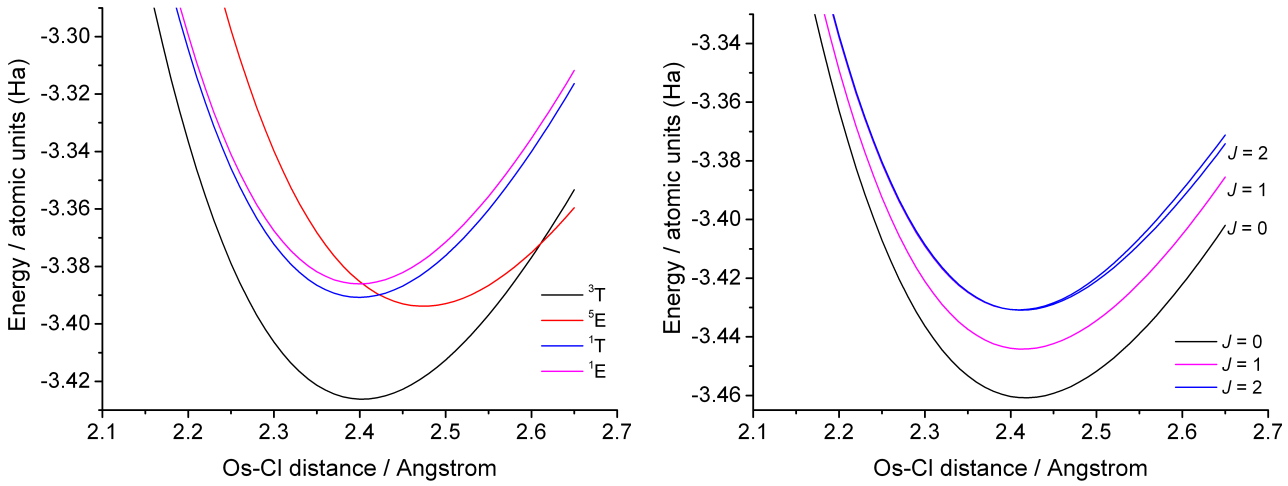

FIG. S4. Evolutions of the total energies of a) the spin terms and of b) the spin-orbital multiplets with the Os-Cl distance in octahedral $[Os^{IV}Cl_6]^{2-}$ anion. All spin states were mixed by spin-orbit coupling in RASSI. Note that at large Os-Cl distance the quintet ^5E becomes the ground state.

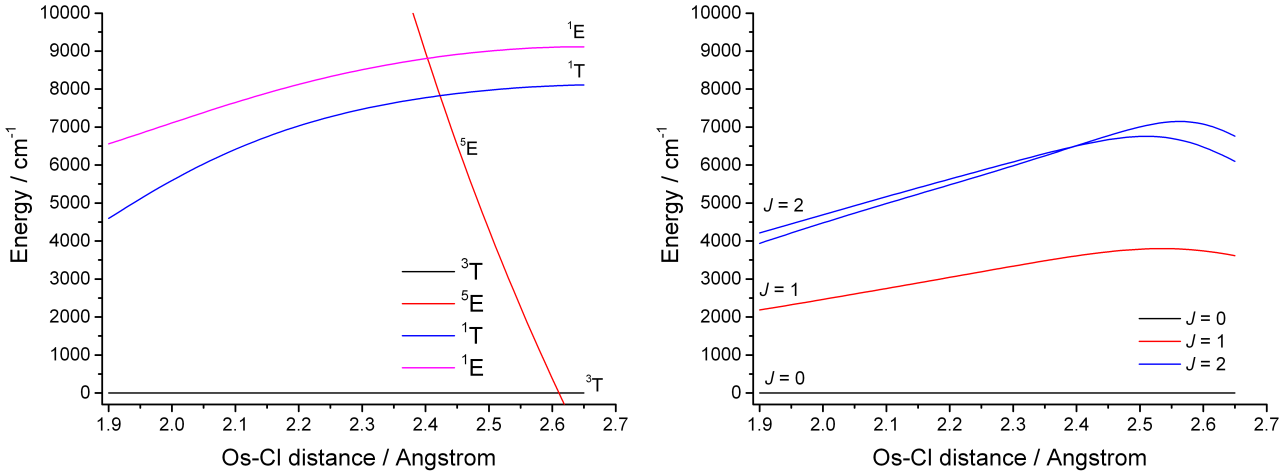

FIG. S5. Evolutions of the relative energies of a) the spin terms and of b) the spin-orbital multiplets with the Os-Cl distance in octahedral $[Os^{IV}Cl_6]^{2-}$ anion. All ligand field spin states were mixed by spin-orbit coupling in RASSI. Note that at large Os-Cl distance the quintet 5E becomes the ground state.

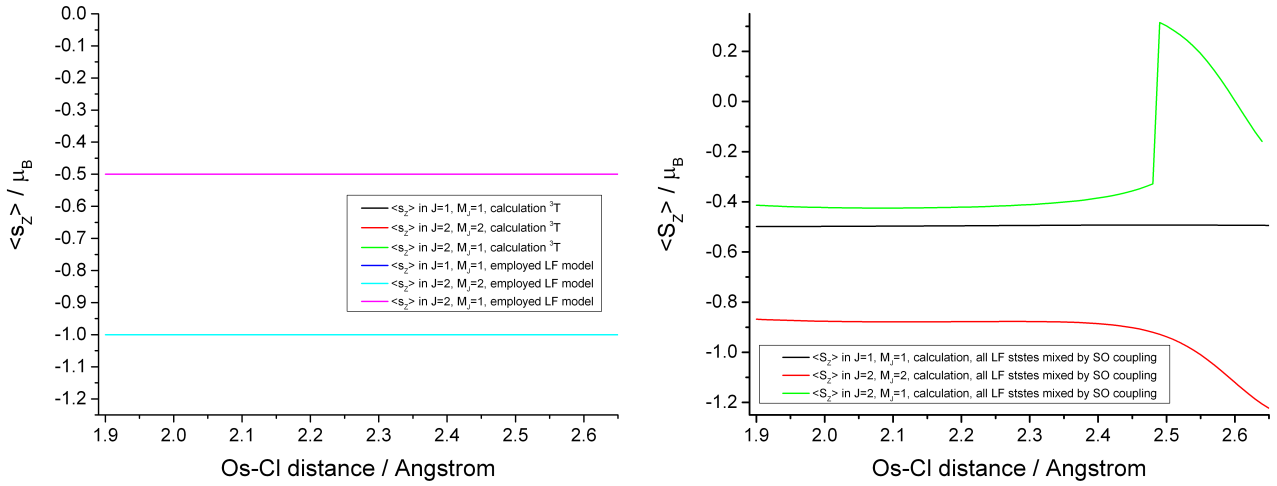

FIG. S6. Evolution of the spin moment in the $J = 1$ and $J = 2$ multiplets in various computational models with the Os-Cl distance in octahedral $[Os^{IV}Cl_6]^{2-}$ anion. Left: only the $^3T_1$ term was mixed by the spin-orbit coupling in RASSI; Right: all ligand field states were mixed by spin-orbit coupling in RASSI.

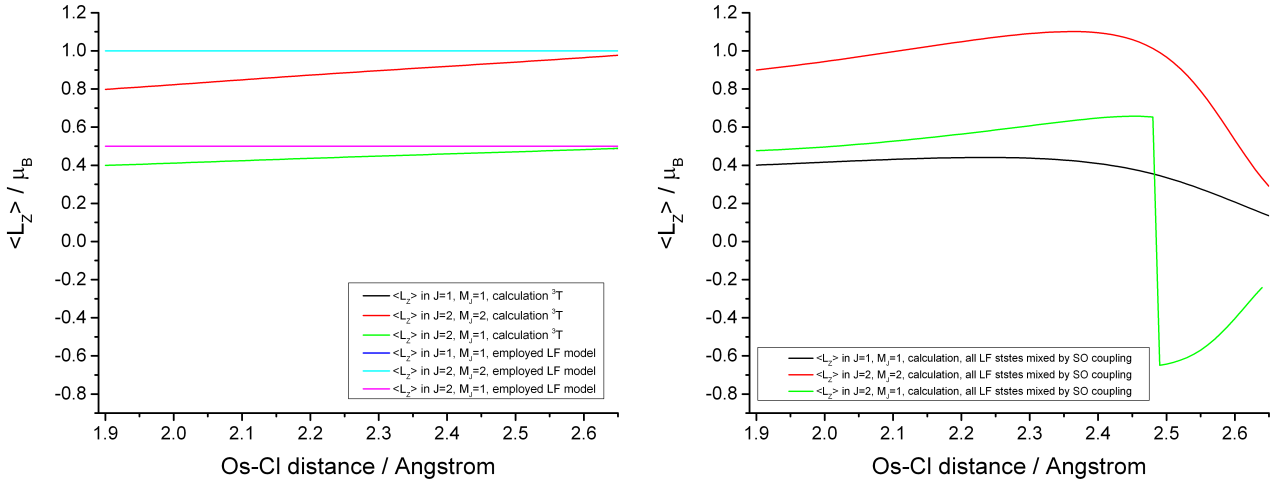

FIG. S7. Evolution of the orbital moment in the $J = 1$ and $J = 2$ multiplets in various computational models with the Os-Cl distance in octahedral $[Os^{IV}Cl_6]^{2-}$ anion. Left: only the $^3T_1$ term was mixed by the spin-orbit coupling in RASSI; Right: all ligand field states were mixed by spin-orbit coupling in RASSI.

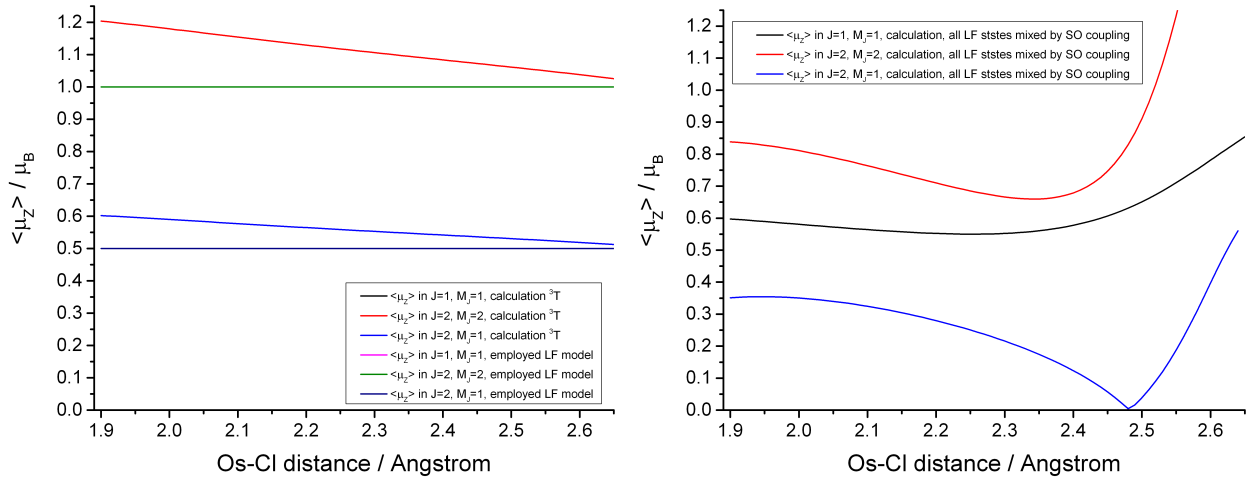

FIG. S8. Evolution of the total magnetic moment in the $J = 1$ and $J = 2$ multiplets in various computational models with the Os-Cl distance in octahedral $[Os^{IV}Cl_6]^{2-}$ anion. Left: only the $^3T_1$ term was mixed by the spin-orbit coupling in RASSI; Right: all ligand field states were mixed by spin-orbit coupling in RASSI.

VI. *AB INITIO* STUDY OF THE AXIALLY DISTORTED OCTAHEDRAL $[OS^{IV}CL_6]^{2-}$ ANION

R_{axial} (Os-Cl)= 2.04957 $\mathring{A}$; $R_{equatorial}$ (Os-Cl)= 2.341695 $\mathring{A}$.

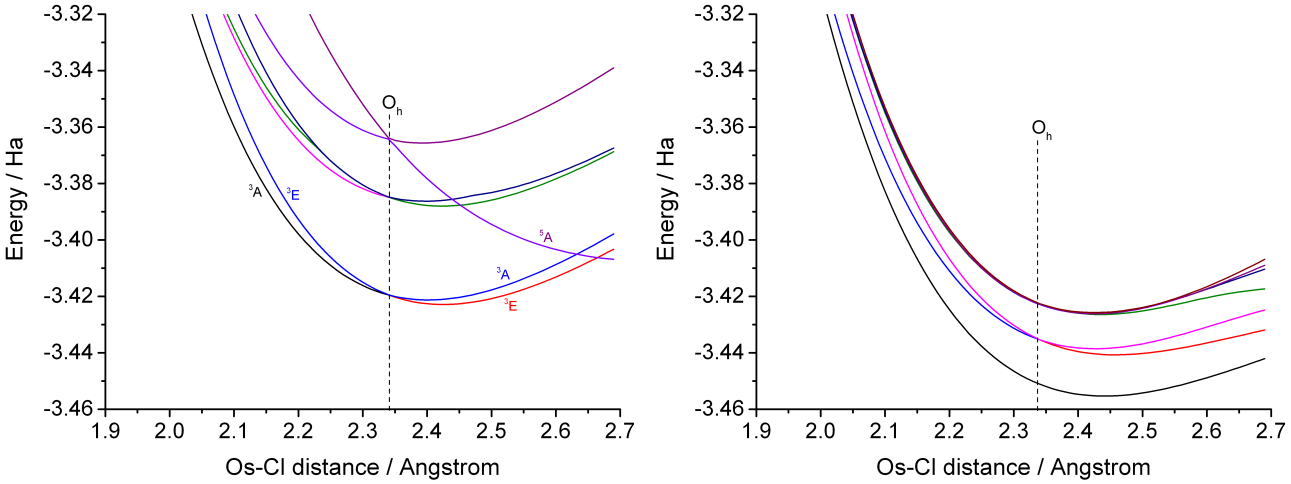

FIG. S9. Evolution of the total energies of a) the spin terms and of b) the spin-orbital multiplets with the Os-Cl distance in axially distorted $[Os^{IV}Cl_6]^{2-}$ anion. All spin states were mixed by spin-orbit coupling in RASSI. Note that at large Os-Cl distance the quintet ^5A becomes the ground state.

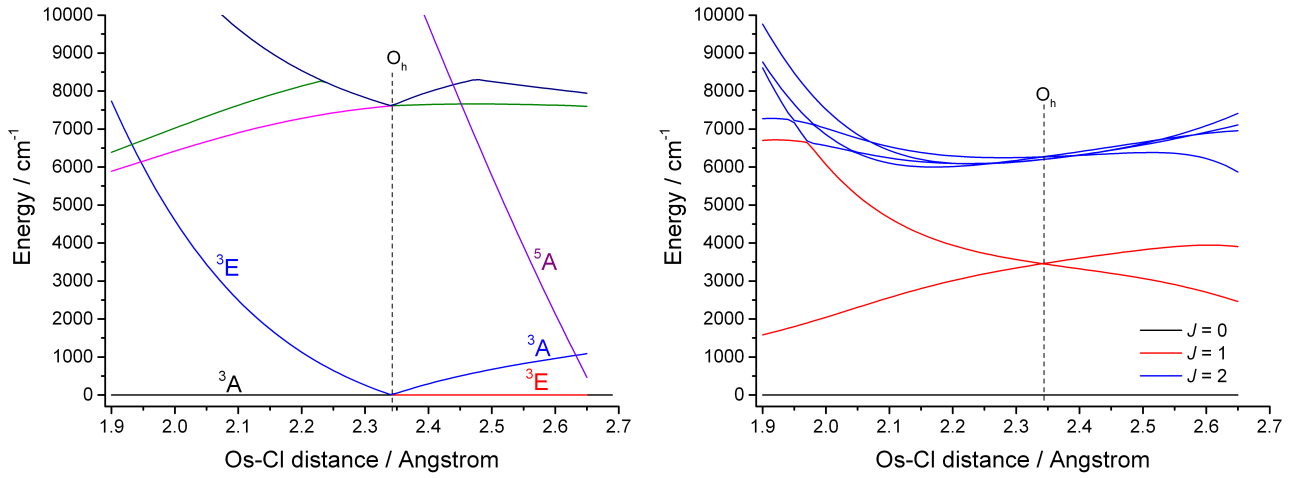

FIG. S10. Evolution of the relative energies of a) the spin terms and of b) the spin-orbital multiplets with the Os-Cl distance in axially distorted $[Os^{IV}Cl_6]^{2-}$ anion. All spin states were mixed by spin-orbit coupling in RASSI. Note that at large Os-Cl distance the quintet ^5A becomes the ground state.

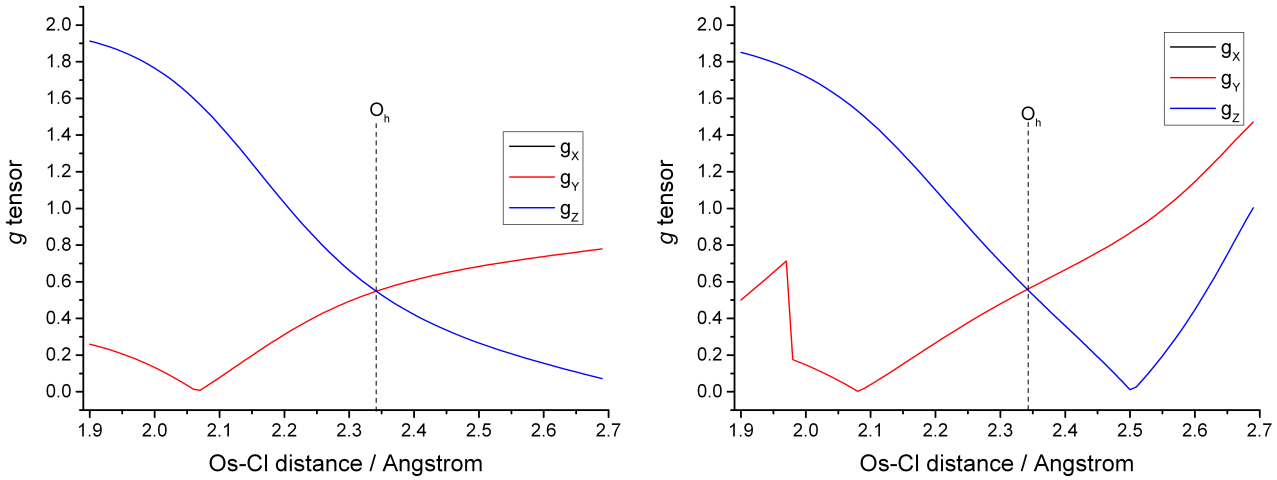

FIG. S11. Evolution of the g tensor of the $J = 1$ multiplet (pseudospin $\tilde{S} = 1$). Left: only roots arising from the octahedral $^3T_1$ term were considered in the spin-orbit coupling in RASSI. Right: all ligand field spin terms were included in the spin-orbit coupling in RASSI.

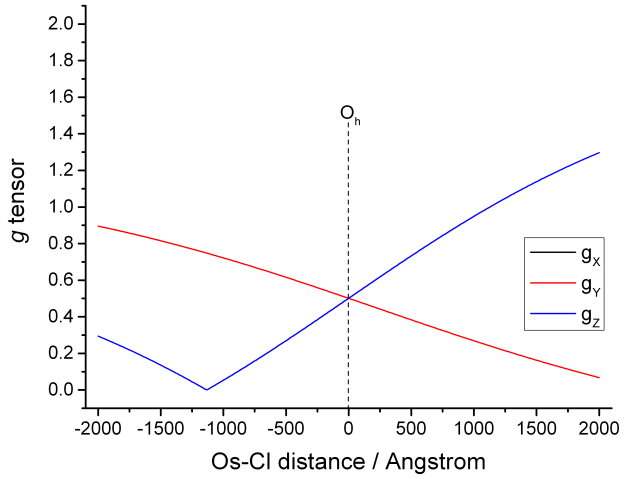

FIG. S12. Evolution of the g tensor of the $J = 1$ multiplet (pseudospin $\tilde{S} = 1$) in the employed ligand field model.

VII. DETAILS OF THE SYNTHESIS OF TRANS-[OS^{IV}CL$_4$(κN$_1$-HIND)$_2$]

The complex was synthesised by solid state Anderson rearrangement reaction,[6] as shown in Scheme S13.

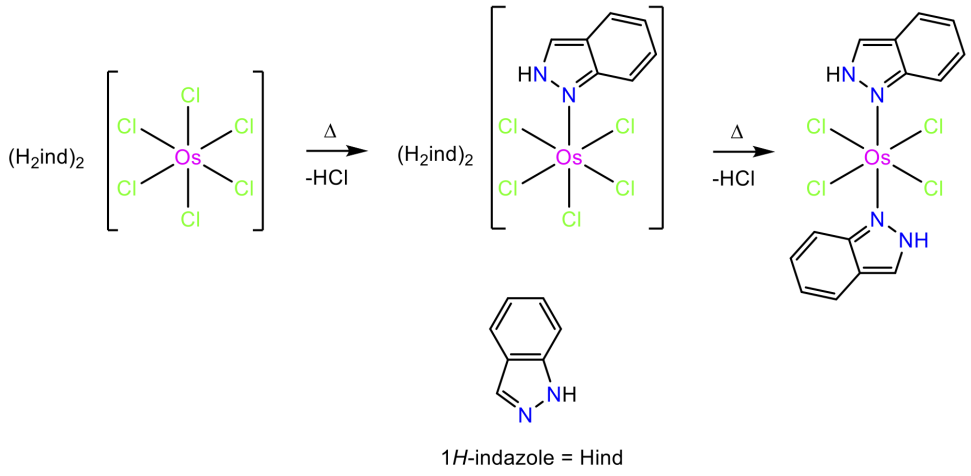

FIG. S13. Solid state synthesis of trans-[Os^{IV}Cl$_4$(κN$_1$-Hind)$_2$].

The intermediate product has been isolated and crystallized as tetrabuthylammonium salt as two isomers with indazole coordinated via both N1 and N2.[7] Synthesis. By heating (H$_2$ind)$_2$[Os^{IV}Cl$_6$] (0.25 mmol) at 150 °C in a glass oven for 45 h followed by a Soxhlet extraction with methanol for 24 h. The dark blue residue collected as a solid from the methanolic extract was re-crystallised from dimethylformamide to give the product in 19% yield.[8]

TABLE S5. Parameters of the decomposition $B_k^q(\alpha)$ of the magnetic moment of $\tilde{J} = 2$. CASSCF/RASSI, AS2 model. This data complements the results presented in Table 3 in the main text.

k	q	α	$B_k^q(\alpha)$
1	-1	X	0.23619329697734E-16
		Y	0.11645212245706E+00
		Z	0.22523788861488E-16
1	0	X	0.12984630331501E-02
		Y	0.97708365607339E-03
		Z	-0.35496012460310E+00
1	+1	X	-0.22233180428829E+00
		Y	-0.10024884793821E-01
		Z	-0.64971720894650E-17
3	-3	X	0.68994158371091E-01
		Y	-0.99414630814041E-01
		Z	-0.19397390825861E-16
3	-2	X	0.12447880681811E+00
		Y	-0.56217874924067E-01
		Z	-0.45178891725152E-17
3	-1	X	0.38372608572310E-17
		Y	0.32855906322688E-01
		Z	0.97267175597157E-17
3	0	X	0.31411462135562E-02
		Y	0.23636888754207E-02
		Z	0.40758529309607E-02
3	+1	X	-0.51316701383806E-01
		Y	-0.55842705976255E-03
		Z	0.79331687287928E-17
3	+2	X	-0.30025939695713E+00
		Y	-0.22683322706206E-01
		Z	0.23339669791242E-17
3	+3	X	-0.63237568441767E-01
		Y	-0.10545965453937E+00
		Z	-0.15666906757344E-17

VIII. FULL DECOMPOSITION OF THE MAGNETIC MOMENT OF THE TRANS-[$OS^{IV}CL_4(\kappa N_1$-HIND)$_2$] AND $\tilde{J} = 2$

Magnetic moment for the $\tilde{J} = 1$ and $\tilde{J} = 2$ is decomposed using irreducible tensor operator technique (ITO). The *ab initio* magnetic moment can be recovered using the equation below:

$$\hat{\mu}_\alpha = \sum_{k=1} \sum_{q=-k}^{k} B_k^q(\alpha) \hat{O}_k^q(J), \tag{S12}$$

where $\hat{O}_k^q(J)$ are odd-ranked Extended Stevens' Operators.[5, 9].

The relatively large values of $B_3^{+2}(X)$, $B_3^{+3}(Y)$, and other values lead to a significant distortion of equidistancy of the Zeeman Splitting of the $\tilde{J} = 2$.

[1] J. S. Griffith, *The Theory of Transition-Metal Ions*, Cambridge University Press, Cambridge, 1971.

[2] B. N. Figgis and M. A. Hitchman, *Ligand Field Theory and Its Applications*, Wiley-VCH, 1999.
[3] A. Abragam and B. Bleaney, *Electron Paramagnetic Resonance of Transition Ions*, Clarendon Press, Oxford, 1970.
[4] O. Kahn, *Molecular Magnetism*, Wiley-VCH, 1993.
[5] L. F. Chibotaru and L. Ungur, *J. Chem. Phys.*, 2012, **137**, 064112.
[6] J. A. Davies, C. M. Hockensmith, V. Y. Kukushkin and Y. N. Kukushkin, *Synthetic Coordination Chemistry: Principles and Practice*, WORLD SCIENTIFIC, 1996, p. 392–396.
[7] G. E. Büchel, I. N. Stepanenko, M. Hejl, M. A. Jakupec, B. K. Keppler, P. Heffeter, W. Berger and V. B. Arion, *J. Inorg. Biochem.*, 2012, **113**, 47–54.
[8] G. E. Büchel, I. N. Stepanenko, M. Hejl, M. A. Jakupec, B. K. Keppler and V. B. Arion, *Inorg. Chem.*, 2011, **50**, 7690–7697.
[9] C. Rudowicz, *Journal of Physics C: Solid State Physics*, 1985, **18**, 1415–1430.